Lawrence Livermore National Laboratory

UCRL-JRNL-203733

Methanol Steam Reformer on a Silicon Wafer

April 20, 2004

H. G. Park, J. Malen, T. Piggott, J.D. Morse, D.A. Sopchak, R. Greif, C.P. Grigoropoulos, M.A. Havstad, R.S. Upadhye

Journal of Microelectromechanical Systems

University of California • P.O. Box 808, L-119 • Livermore, CA 94551 • Ph. 925-423-5864 • FAX 925-422-8277

Methanol steam reformer on a silicon wafer[‡]

Hyung Gyu Park[1], Jonathan Malen[3],W. Thomas Piggott[2], Jeffrey D. Morse[2],
David Sopchak[2], Ralph Greif[1], Costas P. Grigoropoulos[1], Mark Havstad[2],and Ravi Upadhye[2]

[1] Department of Mechanical Engineering, University of California at Berkeley, Berkeley, CA 94720
[2] Center for Micro and Nano Technology, Lawrence Livermore National Laboratory, Livermore, CA 94550
[3] Defense Nuclear Facilities Safety Board, 625 Indiana Ave. NW, Suite 700, Washington, DC 20004

ABSTRACT

A study of the reforming rates, heat transfer and flow through a methanol reforming catalytic micro-reactor fabricated on a silicon wafer are presented. Comparison of computed and measured conversion efficiencies are shown to be favorable. Concepts for insulating the reactor while maintaining small overall size and starting operation from ambient temperature are analyzed.

Keywords: microreactor, heat transfer, methanol reforming

INTRODUCTION

Over the past two decades, there has been increased research in small fuel cells and in miniaturized systems for providing them fuel on demand. Applications include consumer electronics such as cell phones, laptop computers, video camcorders, and radios, as well as military systems such as micro-scale field energy sources for various sensors and remote communication devices.[1]

Several candidate fuels for on-demand generation of hydrogen rich gas have been investigated[2,3] but methanol steam reforming has been preferred due to the lack of inter carbon bonds in methanol, to the limited carbon monoxide production, and to a higher hydrogen fraction in the reformate than that of partial oxidation. A MEMS based micro reformer has the advantages of small features and of integrating many components in a coherent way. Because of these advantages, it is reasonable to expect that micro reformers will be developed for the eventual integration of micro fuel cell systems.

According to Amphlett *et al.*,[4] methanol experiences two overall reactions in a reformer in the presence of $Cu/ZnO/Al_2O_3$ catalyst:

$$CH_3OH + H_2O \underset{k_R'}{\overset{k_R}{\longleftrightarrow}} CO_2 + 3H_2 \qquad (1)$$

$$CH_3OH \xrightarrow{k_D} CO + 2H_2 \qquad (2)$$

Reaction (1), called reforming, is a primary reaction in the methanol steam reforming process. Some portion of the methanol decomposes to produce carbon monoxide via reaction (2). In the presence of water, the three products adjust their compositions via the water-gas shift reaction:

$$CO + H_2O \underset{k_W'}{\overset{k_W}{\longleftrightarrow}} CO_2 + H_2 \qquad (3)$$

For many applications, the reformer working temperature varies from 200 to 300°C, where the dry product composition is such that the proportions of $H_2/CO_2/CO$ are approximately 74/24/2 by volume.

One of the essential issues for reforming for fuel cells is CO contamination. However small, CO always exists in the reformate due to reaction (2), and will poison and ultimately deactivate the Pt catalyzed anode of some fuel cells. Since the poisoning amount of CO is a few tens of ppm, it is very important to estimate accurately the small amount of CO produced. Since a micro reformer operates at a few hundred degrees Celsius, thermal management is also important. Efficient thermal isolation, start-up time and losses are primary considerations in a miniature fuel cell for portable applications.

[‡] Work performed under the auspices of the U.S. Department of Energy by Lawrence Livermore National Laboratory under Contract W-7405-Eng-48.

THEORY

Kinetics

The chemical kinetics of Amphlett *et al.*[4] were used here:

$$\dot{r}_R''' = k_R C_1, \quad \dot{r}_D''' = k_D \tag{4}$$

$$k_R = \bar{k}_R w_{cat}''', \quad k_D = \bar{k}_D w_{cat}''' \tag{5}$$

$$\bar{k}_R = \left[A_R + B_R \ln(\mathrm{SMR})\right] \exp\left[-\frac{E_R}{\bar{R}T}\right] \tag{6}$$

$$\bar{k}_D = A_D \exp\left[-\frac{E_D}{\bar{R}T}\right] \tag{7}$$

Governing equations for a 3 dimensional flow simulation

The conservation equations for the reacting flow inside a reforming bed are:

mass conservation

$$\frac{\partial \rho}{\partial t} + \nabla \cdot (\rho \vec{u}) = 0 \tag{8}$$

momentum conservation

$$\frac{\partial (\rho \vec{u})}{\partial t} + \nabla \cdot (\rho \vec{u}\vec{u}) = \nabla \cdot \mu \nabla \vec{u} - \nabla p + \vec{S}_m(\vec{u}) \tag{9}$$

The Ergun equation[5], neglecting the inertial resistance contribution, was employed to represent the pressure drop:

$$\vec{S}_m(\vec{u}) = -150 \frac{(1-\varepsilon)^2}{\varepsilon^3} \frac{\mu}{D_p^2} \vec{u} \tag{10}$$

energy transport

$$\rho c_v \left(\frac{\partial T}{\partial t} + \nabla \cdot (\vec{u} T) \right) = \nabla \cdot \Gamma \nabla T + S_{CR}, \tag{11}$$

where the thermal conductivity is a volume weighted average of the catalyst bed material ($Cu/ZnO/Al_2O_3$) and the gas mixture.

$$\Gamma = \varepsilon \Gamma_f + (1-\varepsilon)\Gamma_s \tag{12}$$

Endothermic reactions in the reformer result in an energy sink that can be represented as

$$S_{CR} = -\Delta H_R \dot{r}_R''' - \Delta H_D \dot{r}_D''' \tag{13}$$

species transport

$$\frac{\partial \rho_i}{\partial t} + \nabla \cdot (\rho_i u + \vec{j}_i) = r_i \tag{14}$$

Properties such as density, molecular viscosity, and thermal conductivity were calculated assuming an ideal gas mixture. Thus the density was calculated from

$$\rho = \frac{P}{\bar{R}T} M = \frac{P}{\bar{R}T} \sum_i x_i M_i . \tag{15}$$

Wilke's formula[6] was employed to calculate the molecular viscosity and thermal conductivity of an ideal gas mixture.

At the inlet, values of all the variables are assigned:

$$\rho \mathbf{u} = \rho_{in} \mathbf{u}_{in} \qquad m_i = m_{i,in} \qquad T = T_{in} \tag{16}$$

The reactor wall is regarded as no-slip and an impermeable surface:

$$\mathbf{u}\big|_w = 0 \quad \left.\frac{\partial T}{\partial r}\right|_w = 0 \quad \left.\frac{\partial m_i}{\partial r}\right|_w = 0 \tag{17}$$

At the axis of the flow channel, the symmetry boundary condition was applied. Finally, at the outlet, a pressure boundary condition was applied with zero gauge pressure.

Governing equations for a 1 dimensional flow simulation

Three dimensional simulations of reacting porous flows can be computationally expensive, complex and cumbersome for initial scoping of microreactor concepts. A more basic reactor flow analysis has utility for screening micro-reactor concepts, particularly those with porous catalysts. In the axial (flow) direction the plug flow reactor (PFR) species equation is:

$$\sum_{i=1}^{ns} F_{out_{i,j}} - \sum_{i=1}^{ns} F_{in_{i,j}} = r_{i,j} w \Delta x_j$$

$$r_{1,j} = -k_{R,j} c_{1,j} - k_{D,j}$$

$$r_{2,j} = -k_{R,j} c_{1,j} \qquad (18)$$

$$r_{3,j} = k_{R,j} c_{1,j}$$

$$r_{4,j} = k_{D,j}$$

$$r_{5,j} = 3k_{R,j} c_{1,j} + 2k_{D,j}$$

where $F_{i,j}$ is the molar flow rate of species i in the jth PFR cell (which has length Δx_j) $r_{i,j}$ is the reaction rate for species i, c is species concentration and w is the catalyst linear density in kg/m. Solution of the PFR system gives entrance and exit molar flow rates for each cell in the flow channel. The steady flow heat balance on each cell is:

$$\sum_{i=1}^{ns} F_{in_{i,j}} h_{in_{i,j}} = \sum_{i=1}^{ns} F_{out_{i,j}} h_{out_{i,j}} + Q_j^{rxn} - Q_j^{convn} \qquad (19)$$

The summation terms give the enthalpy flows. The heat produced or removed by the progress of the chemical reaction in the system is determined by the solution to the PFR species equations and the heats of reaction. The convection transport term defines the coupling between the fluid flow channel and the surrounding solid material (Si wafer). Here we use a convection correlation developed for packed beds[7]:

$$Q_j^{convn} = h_j^{bed} * (T_j - T_j^{surr}) * A_j^{surr}$$

$$h_j^{bed} = C_1 * \mathrm{Re}_j^{C_2} \frac{k}{D_{part}}$$

$$T_j^{surr} = [\sum_{nc=1}^{N_j} T_{j,nc}^{facet} * A_{j,nc}^{facet}] / A_j^{surr} \qquad (20)$$

$$A_j^{surr} = \sum_{nc=1}^{N_j} A_{j,nc}^{facet}$$

Reynolds number is based on particle diameter and average velocity in each PFR cell. The N_j facets bounding PFR cell j are used to compute the surrounding temperature T^{surr}_j and surrounding area, A^{surr}_j, for convective heat transfer.

These PFR relations were coupled to three dimensional finite element conduction calculations (in TOPAZ3D[8]) by a nonlinear heat flux boundary condition: at each time step the conduction equation is solved until the temperature and reaction rate dependent heat load term converges. Heat loss from the solid to the surroundings has been modeled with a free convection heat transfer coefficient, h_{fc}, or with a radiative transport coefficient, $\mathcal{F}$:

$$q = \mathcal{F}\sigma(T^4 - T_\infty^4) \qquad (21)$$

where $\mathcal{F}$ is determined by material emittances and shield number.

Serpentine micro reactor

The micro reformer considered here is a serpentine shape of 7 passes each 1 mm wide etched in a silicon substrate (Fig. 1) to 500μm depth. $Cu/ZnO/Al_2O_3$ catalyst fills the channel, and two electric heaters on the back side of the substrate (Fig. 2) supply the required amount of heat into the channel across the silicon substrate. A Pyrex glass panel covers the packed bed channel and the rest of the substrate front surface. Liquid methanol-water mixture at room temperature enters the channel inlet to travel through the evaporator zone equipped with the first heater. The vaporized methanol-water gas mixture enters the packed-bed catalytic reaction zone at 100°C where hydrogen, carbon dioxide and carbon monoxide are formed. The second heater is patterned on the back side of the Si substrate opposite the packed bed portion of the etched channel.

The reformer was fabricated and tested with the above channel etched in a 2.54cm×2.54cm×1.mm silicon substrate and a 0.5mm thick Pyrex glass cover. In the fully three dimensional flow model (using FLUENT[9]) the glass cover was replaced by a one-dimensional thermal resistance boundary condition to reduce model size and computing time. The domain was divided into 33,000 fluid cells for the channel and 135,000 solid cells for the substrate. For the one dimensional flow modeling (using TOPAZ3D) both the silicon substrate and the pyrex cover were modeled (44,445 solid elements) and the PFR consisted of 137 axial locations coupled to the 6031 finite element facets of the flow channel surface (visible in Figure 1).

For both the FLUENT and TOPAZ3D modeling, conjugate heat transfer at the interface of the fluid channel and the solid substrate is obtained by equating the heat fluxes from the fluid and solid sides.

The catalyst loading was 53.1mg into the packed bed volume of 5.0×10^{-8} m^3. At the inlet to the bed the mass flow rate is 1.43×10^{-7} kg/s, temperature is 100°C, and the steam-to-methanol molar ratio is 1.1. The inlet mass flow rate

corresponds to the liquid input of 10μL/min at 20°C. The boundary condition on the Si substrate under the bed heater is a constant heat flux corresponding to 2 to 4 W of Joule heating (depending on the heat loss boundary condition specified to the remaining exterior surfaces of the Si and glass as discussed below).

Two forms of thermal isolation are considered here. Low thermal conductivity solid insulations are perhaps the simplest option but only for the most exotic and difficult to handle materials (low conductivity evacuated aerogels) is performance approaching adequate. Highly reflective radiative shields separated by thin evacuated gaps are potentially superior but more complex, expensive and difficult to implement. Using simple one dimensional heat transfer relations we compare these two options (Fig. 3) for the design at hand: a one inch square wafer operating at 250 Celsius which is producing reformate for a 2 to 3 watt fuel cell. Steady state heat loss from the two sides of such a wafer should be 0.2 to 0.3 watts or less. Further, a requirement of military systems is sometimes an exterior temperature of less than 40 Celsius to limit thermal signature. Both the 3 and 4 shield cases satisfy the low temperature and low heat loss criteria but the graph presents idealized results in the sense that shield gap is infinitesimal and conductive transport is zero. In practice some contact will occur and real gap sizes enhance heat loss. The effect of these two mechanisms is to move up and to the left from the radiative curve shown toward the conduction curve.

RESULTS

Figure 4 compares measurements and calculations of outlet flow rate for four inlet flow rates and a wide range of temperatures. Since Amphlett[4] kinetics were based on tests from 200 to 260°C it is not surprising to see a little disagreement at the higher temperatures. For design work this is deemed adequate.

Results for various grid and time step sizes are given in table 1. There is no significant dependence of the results on time step size, which varies over 4 orders of magnitude. Finite element grid coarsening (from 44445 to 9524 elements) was not accompanied by comparable PFR coarsening (from 137 to 118) because the PFR grid was already coarse. Assessment of the adequacy of the PFR grid should be based on a comparison to the FLUENT modeling (postponed until fig. 6).

Figure 5 shows the steady thermal profile of the exterior of the silicon wafer for a radiatively shielded ($\mathcal{F}$=0.05) case. Temperatures are elevated on the surface of the microchannel despite the endothermic heat of reaction because the I^2R heating is applied over the microchannel on the backside of the channel (as seen in Fig. 2). In an absolute sense, thermal gradients are small (< 3 K) due to the high thermal conductivity of Si (148. w/(mK).

The one and three dimensional approaches to the flow simulation are contrasted in figures 6 and 7. Molar flow rates for the FLUENT calculations are averages over the flow channel at the reactor exit while those from TOPAZ3D are the values for the last PFR centroid before exhausting from the chip. The discrepancy between hydrogen flow rates at long times (>250 seconds) is greater than the corresponding discrepancy in methanol flow rate by the reforming stoiciometry. Figure 7 shows that errors in both methanol and hydrogen flow rates are modest for reasonable reactor lengths. Very short reactor lengths are not practical and the hydrogen error starts out very large because hydrogen flow is initially zero.

Comparison of thermal isolation options is summarized in Table 2. Insulating with polyimide foam or evacuated silicon powder is viable in that these materials are available but exterior surface temperatures are too high (172 °C for Kapton and 83 °C for Si powder) given the practical thicknesses we have posed. Comparison of the radiatively insulated options shows the level of benefit accrued in exchange for reducing the radiative transport by adding shields or decreasing shield emissivity. Cheap and simple means of obtaining low emissivity and negligible conduction are being sought.

Figure 8 gives the transient reactor performance with a radiatively shielded ($\mathcal{F}$=0.05) insulation package. Reduction of system thermal mass, increased battery capacity or burning the unreformed fuel are options for reducing start-up time. Figure 9 gives the transient behavior of reactor conversion efficiency and fluid exit temperature. Given the form of the conversion efficiency transient there are some fuel cells which could begin operation at 10 to 15 seconds given this reformate product.

ACKNOWLEDGMENTS

This work was performed under the auspices of the U. S. Department of Energy by the University of California, Lawrence Livermore National Laboratory under Contract No. W-7405-Eng-48.

REFERENCES

[1] Morse, J. D., Jankowski, A. F., Graff, R. T., and Hayes, J. P., *J. Vac. Sci. Technol. A*, 18(4), Jul/Aug 2000

[2] Brown, L. F., *Int. J. Hydrogen Energy*, 26, pp. 381-397, 2001

[3] Joensen, F. and Rostrup-Nielsen, J. R., *J. Power Sources*, 105, pp. 195-201, 2002

[4] Amphlett, J.C. *et. al*., "Hydrogen production by steam reforming of methanol for polymer electrolyte fuel cells," International Journal of Hydrogen Energy, Vol. 19, No. 2, pp131-137,1994

[5] Ergun, S., Chemical Engineering progress, 48(2), pp. 89-94,1952

[6] Mills, A. F., *Mass Transfer*, Prentice-Hall Inc., 2001

[7] Azbel, D., Fundamentals of Heat Transfer for Process Engineering, Noyes Publications, 1984

[8] Shapiro, A.B., "TOPAZ3D—A Three Dimensional Finite Element Heat Transfer Code," University of California, Lawrence Livermore National Laboratory, Rept. UCID-20484, 1985.

[9] *Fluent User Guide v6*, Fluent Inc., 2001

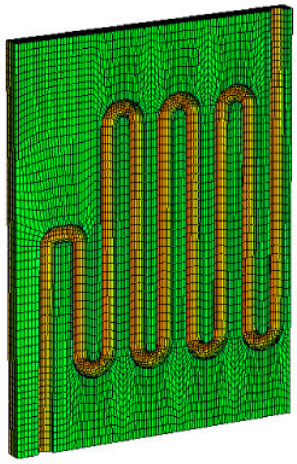

Figure 1. Finite element mesh of silicon wafer with etched microchannel for packed bed reactor.

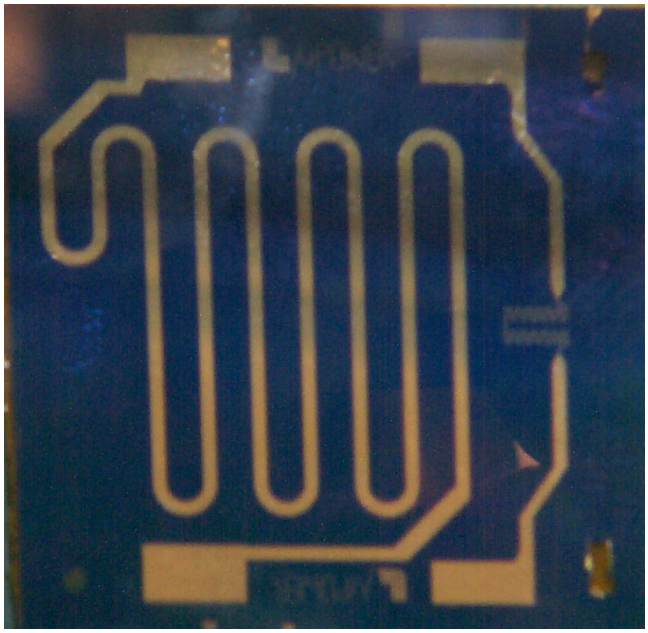

Figure 2. Silicon wafer with 2 Pt resistance heaters deposited on back face. The right and left heaters are under the fuel evaporation and reforming regions respectively.

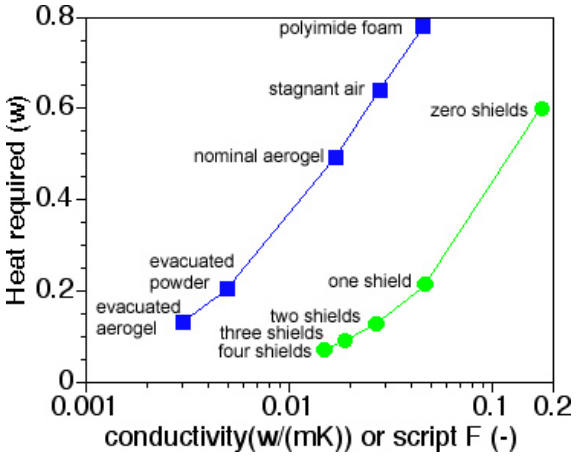

Figure 3. Comparison of conductive and radiative insulation options. See Eqn. 21 for defn. of script F.

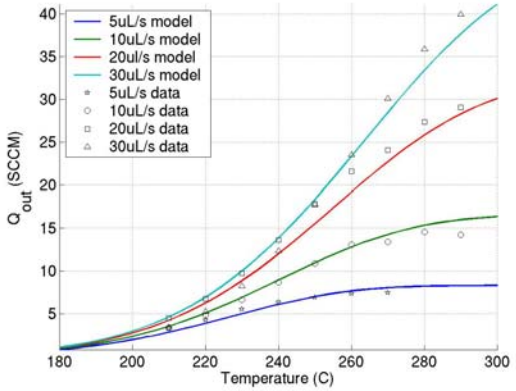

Figure 4. Comparison of computed and measured output volumetric flow rate as a function of temperature for four reactor flow rates.

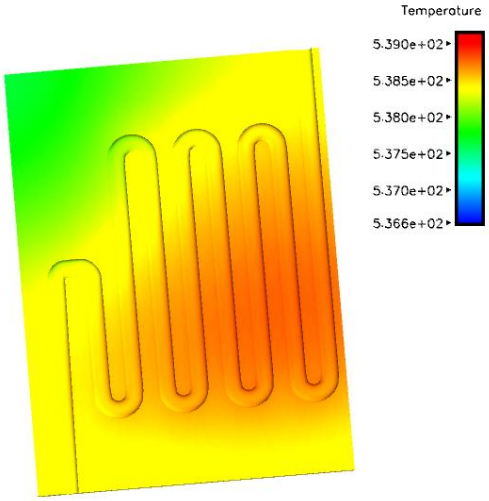

Figure 5. Thermal profile of wafer surface during steady state operation. Temperatures are in Kelvin.

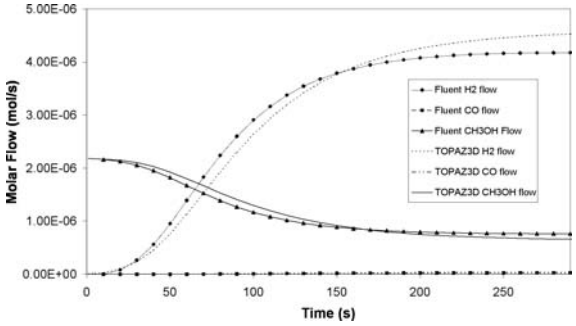

Figure 6. Comparison of FLUENT and TOPAZ3D reactor simulations.

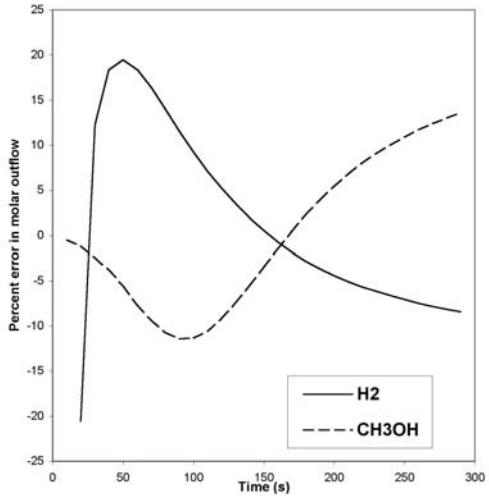

Figure 7. Error in hydrogen and methanol outflow calculation by PFR in TOPAZ3D relative to three dimensional FLUENT calculation.

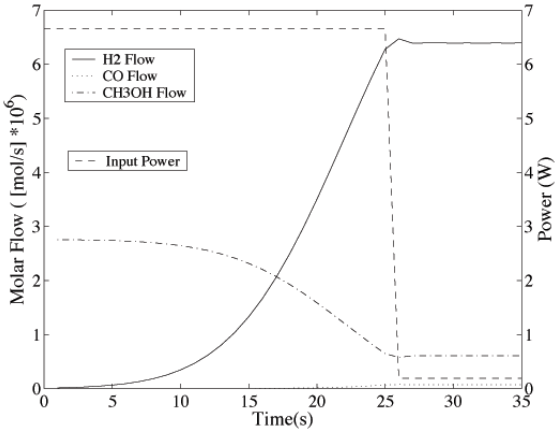

Figure 8. Reactor start-up transient: molar flows and input heater power.

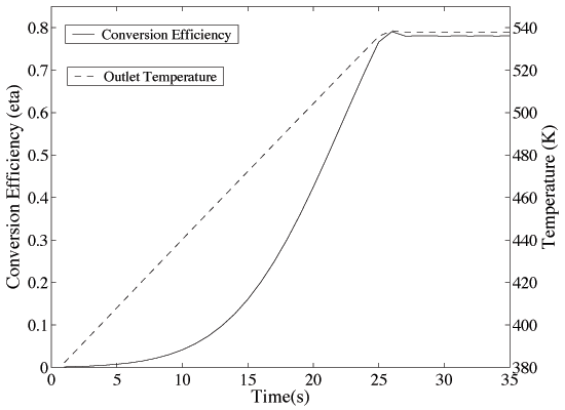

Figure 9. Reactor start-up transient: temperature and conversion efficiency

# of Finite Elements	# of PFR Elements	Δt (s)	Outlet T (K)	Outlet H_2 Flow (mol/s)	Outlet CO Flow (mol/s)	Outlet CH_3OH Flow (mol/s)	η
44445	137	5	385.5	1.540E-8	4.158E-12	2.755E-6	1.860E-3
44445	137	2.5	385.7	1.570E-8	4.269E-12	2.755E-6	1.896E-3
44445	137	1	385.9	1.586E-8	4.332E-12	2.755E-6	1.916E-3
44445	137	0.1	386.0	1.596E-8	4.367E-12	2.755E-6	1.928E-3
44445	137	0.01	386.0	1.597E-8	4.370E-12	2.755E-6	1.929E-3
44445	137	0.001	386.0	1.597E-8	4.371E-12	2.755E-6	1.929E-3
44445	118	1	385.9	1.582E-8	4.323E-12	2.755E-6	1.912E-3
44445	118	0.1	386.0	1.592E-8	4.357E-12	2.755E-6	1.923E-3
44445	118	0.01	386.0	1.593E-8	4.361E-12	2.755E-6	1.924E-3
44445	118	0.001	386.0	1.593E-8	4.361E-12	2.755E-6	1.924E-3
9524	118	1	385.7	1.554E-8	4.216E-12	2.755E-6	1.877E-3
9524	118	0.1	385.8	1.563E-8	4.250E-12	2.755E-6	1.888E-3
9524	118	0.01	385.8	1.564E-8	4.253E-12	2.755E-6	1.889E-3
9524	118	0.001	385.8	1.564E-8	4.254E-12	2.755E-6	1.890E-3

Table 1: Grid and Time Step Test to 5 s

Run	Energy used to time τ (J)	CH_3OH Used (mol $*10^5$)	τ (s)	H_2 Produced (mol $*10^5$)	Outflow Temp. (K)	Maximum Exterior Temp. at Steady State (K)	Steady State Heat Input (W)
F=0.03	153.2	6.348	23	2.980	524.1	540	0.113
F=0.05	153.2	6.348	23	2.937	523.3	540	0.188
F=0.1	159.8	6.624	24	3.362	527.5	540	0.375
F=0.2	166.5	6.900	25	3.672	529.2	539	0.745
F=0.3	166.5	6.900	25	3.413	524.9	539	1.1156
Polyimide Foam, 5 mm	173.2	7.176	26	3.927	528.8	445	1.029
Silicon Powder, 1 mm	159.8	6.624	24	3.373	528.1	356	0.199

Table 2. Runs to time τ where η=0.7